ISSN: 0067-2904

Investigation of Ground Density Distributions and Charge Form Factors for ^{14,16,18,20,22}N using Cosh Potential

Safana S. Odah*, Arkan R. Ridha
Department of Physics, College of Science, University of Baghdad, Baghdad-Iraq

Received: 14/8/2021 Accepted: 14/2/2022 Published: 30/9/2022

Abstract:
The bound radial wave functions of Cosh potential which are the solutions to the radial part of Schrodinger equation are solved numerically and used to compute the size radii; i.e., the root-mean square proton, neutron, charge and matter radii, ground density distributions and elastic electron scattering charge form factors for nitrogen isotopes ^{14,16,18,20,22}N. The parameters of such potential for the isotopes under study have been opted so as to regenerate the experimental last single nucleon binding energies on Fermi's level and available experimental size radii as well.
PACS number(s): 21.10.Ft, 21.60.Cs, 21.10.Gv, 25.30.Bf

Keywords: Nitrogen isotopes, Cosh potential, density distributions, charge form factors, size radii

تحقيق توزيعات الكثافة الأرضية وعوامل التشكل الشحنية لنظائر النايتروجين ^{14,16,18,20,22}N باستخدام جهد كوش

سفانة سعد عودة* و أركان رفعت رضا
قسم الفيزياء، كلية العلوم، جامعة بغداد، ، بغداد، العراق

الخلاصة
تم حل الدوال الموجية القطرية المقيدة لجهد كوش والتي هي حلول للجزء القطري لمعادلة شرودنكر عدديا واستخدمت لحساب الانصاف الاقطار النووية؛ معدل نصف القطر البروتوني والنيوتروني والشحني والكتلي، وتوزيعات الكثافة الارضية وعوامل التشكل الشحنية للاستطارة الالكترونية لنظائر النايتروجين ^{14,16,18,20,22}N. معلمات مثل هذا الجهد للنظائر تحت الدراسة اختيرت بحيث تولد طاقات الربط العملية للنيوكليون الاخير على سطح فيرمي وايضا الانصاف الاقطارالنووية العملية المتوفرة.

Introduction

In the nuclear realm, choosing the right nuclear potential is of great importance [1]. Firstly, the harmonic-oscillator (HO) potential is widely utilized potential for theoretical nuclear applications. It has a restricted application since $V(r)$ approaches to infinity at large r besides, the radial wave functions (WF) of HO are mainly characterized by Gaussian fall off

*Email: safana.oada1204@sc.uobaghdad.edu.iq

behavior (steep slope behavior) [2-4]. To improve the performance of the WFs of HO potential, changes are required; in Refs [5-7], the two-frequency shell model approach were used with limited success to study the exotic nuclei. In Refs [8-10] the transformed HO WFs in local scale transformation (LST) were successfully used to regenerate the tail characteristic in the density distribution for exotic nuclei, which explained the experimental ground data quite well. Furthermore, the WSs of the Woods-Saxon (WS) potential have been used to compute bulk properties of stable and exotic nuclei [11-13].

In the present work, the radial part of the Schrödinger equation was solved numerically and the wave functions have been tested by calculating the ground properties of nitrogen isotopes; ^{14,16,18,20,22}N (size radii, density distributions and ground electron scattering formation factors). The adopted parameters of Cosh potential are chosen to reproduce the last single proton and neutron binding energies near the Fermi's level.

Theoretical bases

The Schrodinger equation for a single nucleon in A-nucleon system is given by [14]

$$\left[-\frac{\hbar^2}{2\mu}\vec{\nabla}^2 + U(r)\right]\psi_{nljt_z}(r,\theta,\varphi) = E_{nljt_z}\psi_{nljt_z}(r,\theta,\varphi) \quad (1)$$

The Cosh form of $U(r)$ which is symmetrized form of WS potential and can be written as [15]

$$f(r,R,a) = \frac{1+\cosh\left(\frac{R}{a}\right)}{\cosh\left(\frac{r}{a}\right)+\cosh\left(\frac{R}{a}\right)} \quad (2)$$

where $R = r_0(A-1)^{1/3}$ and a are the radius (of the system, $A-1$) and diffuseness of the potential, correspondingly. $\mu = \frac{m(A-1)}{A}$ is the reduced mass for the single nucleon and the rest of $(A-1)$ system. In Eq. (1), the wave function, $\psi_{nljt_z}(r,\theta,\varphi)$ can be written as [14]

$$\psi_{nljt_z}(r,\theta,\varphi) = R_{nljt_z}(r)Y_{jm}(\theta,\varphi)\chi_{ss_z}\chi_{tt_z} \quad (3)$$

$Y_{jm}(\theta,\varphi)$, χ_{ss_z} and χ_{tt_z} represent the spherical harmonics, spinor for spin and isospin wave functions, correspondingly.

The nuclear potential, $U(r)$ in Eq. (1) can be written as the sum of central, spin-orbit and Coulomb parts [14]

$$U(r) = U_c(r,R,a) + U_{s.o.}(r,R_{s.o.},a_{s.o.}) + U_{coul.}(r) \quad (4)$$

where

$$U_c(r,R,a) = -V_0 f(r,R,a)$$

$$U_{s.o.}(r,R_{s.o.},a_{s.o.}) = 2\frac{V_{s.o.}}{r}\frac{df(r,R,a)}{dr}\langle\hat{l}.\hat{\sigma}\rangle$$

$$\langle\hat{l}.\hat{\sigma}\rangle = \begin{cases} -\frac{1}{2}(l+1) & for\ j = l-\frac{1}{2} \\ \frac{1}{2}l & for\ j = l+\frac{1}{2} \end{cases}$$

and

$$U_C(r) = \begin{cases} \begin{cases} (Z-1)\frac{e^2}{r} & if\ r > R_C \\ \frac{(Z-1)e^2}{2R_C}\left[3-\left(\frac{r}{R_C}\right)^2\right] & if\ r < R_C \end{cases} & for\ protons \\ 0 & for\ neutrons \end{cases}$$

V_0 and $V_{s.o.}$ are the depth of the central and spin-orbit potentials. The radial part of Schrodinger's equation can be reduced to,

$$\frac{1}{r^2}\frac{d}{dr}\left(r^2\frac{dR_{nljt_z}(r)}{dr}\right)+\frac{2\mu}{\hbar^2}\left[E_{nlj,t_z}-\frac{l(l+1)\hbar^2}{2\mu r^2}-U(r)\right]R_{nljt_z}(r)=0$$

The use of such potential give the radial and angular parts which can be used to calculate the proton/neutron density distributions given by [5],

$$\rho_{J,t_z}(r)=\frac{1}{\sqrt{4\pi(2J_i+1)}}\sum_{a,b}\chi_{a,b}^{J_i,J_f,t_z}\langle j_b\|Y_J\|j_a\rangle R_{n_al_aj_at_z}(r)R_{n_bl_bj_bt_z}(r) \qquad (4)$$

The matter density can be accounted from [16,17],

$$\rho_{J,m}(r)=\rho_{J,t_z=p}(r)+\rho_{J,t_z=n}(r) \qquad (5)$$

The charge electron scattering form factors is a Fourier transform to Eq. (4) [16],

$$F_{J,t_z}(q)=\frac{4\pi}{qZ}\int_0^\infty \rho_{J,t_z}(r)\sin(qr)\,rdr \qquad (6)$$

Finally, the size radius for proton, neutron and matter is denoted by $\langle r^2\rangle_g^{\frac{1}{2}}$ and computed from [16],

$$\langle r^2\rangle_g^{\frac{1}{2}}=\sqrt{\frac{4\pi}{g}\int_0^\infty \rho_{J,t_z}(r)r^2dr} \qquad (7)$$

The $\langle r^2\rangle_{ch}^{\frac{1}{2}}$ is related to the $\langle r^2\rangle_p^{\frac{1}{2}}$ by [16],

$$\langle r^2\rangle_{ch}^{\frac{1}{2}}=\sqrt{\langle r^2\rangle_p+0.64} \qquad (8)$$

Result and discussions

The pure configuration with independent particle model (IPM) are applied with Cosh potential to ^{14,16,18,20,22}N to calculate the size radii, density distributions and charge form factors.

The six parameters of Cosh potential, V_0, r_0, a, V_{so}, $r_{0(so)}$ and a_{so} are adjusted so as to regenerate the available experimental single nucleon binding energies and rms radii for nuclei under study. In Table 1, the parameters of the potential for ^{14,16,18,20,22}N are listed. The procedure of chosen such parameters in Table 1 are done by fixing the values of the parameters R_C, r_0 and $r_{0(so)}$ to be equal, besides The V_{so} is always chosen to be 9.0 MeV, therefore, the zone of parameters would be limited to the three parameters V_0, r_0 and a. Such three parameters play crucial role in the present work. In tables from 2 to 6, the calculated single-nucleon binding energies are computed using Cosh potentials for Nitrogen isotopes (^{14,16,18,20,22}N).

Table 1- Cosh potential parameters for ^{14,16,18,20,22}N. $R_C=r_0=r_{0(so)}$

$^{14}_{7}N_7$	Neutron binding energy (MeV)	Exp. neutron binding energy (MeV) [18,19]	Proton binding energy (MeV)	Exp. proton binding energy (MeV) [18,19]
$1s_{1/2}$	30.236	-	28.673	-
$1p_{3/2}$	16.455	-	14.083	-
$1p_{1/2}$	10.553	10.55338 ± 0.00027	7.550	7.55056 ± 0

Table 2-Single-nucleon binding energies for $^{14}_{7}N_{7}$

$^{A}_{Z}X_{N}\,(J^{\pi}T)$ [18,19]	$t_{1/2}$ [18,19]	n/p	V_0	r_0	a	V_{so}	$r_{0(so)}$	a_{so}
$^{14}_{7}N_{7}(1^{+}0)$	Stable	n	50.030	1.300	0.50	9.0	1.300	0.50
		p	53.693	1.240	0.45	9.0	1.240	0.45
$^{16}_{7}N_{9}(2^{-}1)$	$7.13 \pm 0.02\ s$	n	46.989	1.250	0.39	9.0	1.250	0.39
		p	54.828	1.220	0.35	9.0	1.220	0.35
$^{18}_{7}N_{11}(1^{-}2)$	$619.2 \pm 1.9\ \mu s$	n	54.883	1.220	0.45	9.0	1.220	0.45
		p	52.670	1.300	0.42	9.0	1.300	0.42
$^{20}_{7}N_{13}(\text{unknown}\frac{5}{2})$	$136 \pm 3\ \mu s$	n	42.180	1.200	0.36	9.0	1.200	0.36
		p	54.174	1.275	0.39	9.0	1.275	0.39
$^{22}_{7}N_{15}(0^{-}4)$	$24 \pm 5\ \mu s$	n	39.649	1.314	0.40	9.0	1.314	0.40
		p	56.194	1.263	0.40	9.0	1.263	0.40

Table 3-Single-nucleon binding energies for $^{16}_{7}N_{9}$

$^{16}_{7}N_{9}$	Neutron binding energy (MeV)	Exp. neutron binding energy (MeV) [18,19]	Proton binding energy (MeV)	Exp. proton binding energy (MeV) [18,19]
$1s_{1/2}$	29.120	-	32.074	-
$1p_{3/2}$	15.823	-	17.652	-
$1p_{1/2}$	9.885	-	11.478	11.47821±0.00244
$1d_{5/2}$	2.488	2.48885 ± 0.0023	-	-

Table 4-Single-nucleon binding energies for $^{18}_{7}N_{11}$

$^{18}_{7}N_{11}$	Neutron binding energy (MeV)	Exp. neutron binding energy (MeV) [18,19]	Proton binding energy (MeV)	Exp. proton binding energy (MeV) [18,19]
$1s_{1/2}$	35.909	-	32.731	-
$1p_{3/2}$	21.815	-	20.067	-
$1p_{1/2}$	16.206	-	15.205	15.20658±0.02542
$1d_{5/2}$	7.411	-	-	-
$2s_{1/2}$	2.828	2.82822±0.02387	-	-

Table 5-Single-nucleon binding energies for $^{20}_{7}N_{13}$

$^{20}_{7}N_{13}$	Neutron binding energy (MeV)	Exp. neutron binding energy (MeV) [18,19]	Proton binding energy (MeV)	Exp. proton binding energy (MeV) [18,19]
$1s_{1/2}$	26.352	-	35.007	-
$1p_{3/2}$	14.308	-	22.486	-
$1p_{1/2}$	8.802	-	17.936	17.93647±0.11301
$1d_{5/2}$	2.161	2.16173±0.05796	-	-

Table 6-Single-nucleon binding energies for $^{22}_{7}N_{15}$

$^{22}_{7}N_{15}$	Neutron binding energy (MeV)	Exp. neutron binding energy (MeV) [18,19]	Proton binding energy (MeV)	Exp. proton binding energy (MeV) [18,19]
$1s_{1/2}$	25.118	-	40.224	-
$1p_{3/2}$	16.501	-	28.373	-
$1p_{1/2}$	13.390	-	24.707	20.894±0.444
$1d_{5/2}$	7.346	-	-	-
$2s_{1/2}$	2.734	-	-	-
$1d_{3/2}$	0.731	1.28381±0.21443	-	-

In Table 7, the available experimental and computed size radii for ^{14,16,18,20,22}N are presented. Very good agreement with experimental data for all Nitrogen isotopes are obtained.

Table 7-Calculated and experimental size radii for ^{14,16,18,20,22}N

${}^{A}_{Z}X_{N}$	Calculated $\langle r^2\rangle_p^{1/2}$	Exp. $\langle r^2\rangle_p^{1/2}$ [20]	Calculated $\langle r^2\rangle_n^{1/2}$	Exp. $\langle r^2\rangle_n^{1/2}$ [21]	Calculated $\langle r^2\rangle_{ch}^{1/2}$	Exp. $\langle r^2\rangle_{ch}^{1/2}$ [22]	Calculated $\langle r^2\rangle_m^{1/2}$	Exp. $\langle r^2\rangle_m^{1/2}$
${}^{14}_{7}N_{7}$	2.445	2.43(4)	2.518	-	2.549	2.540(20)	2.482	2.50(3) [20]
${}^{16}_{7}N_{9}$	2.384	-	2.640	2.64(16)	2.483	-	2.531	2.53(14) [23]
${}^{18}_{7}N_{11}$	2.531	2.53(3)	2.765	-	2.619	-	2.676	2.68(2) [20]
${}^{20}_{7}N_{13}$	2.522	2.52(3)	2.995	-	2.604	-	2.838	2.84(5) [20]
${}^{22}_{7}N_{15}$	2.530	2.53(3)	3.307	-	2.606	-	3.081	3.08(12) [20]

Figure 1(a) and (b), the calculated and the experimental CDDs as well as the the calculated and the experimental charge form factors for ^{14}N are respectively depicted. The solid curves represent the calculations using Cosh potential. The dotted symbols represent experimental data. It is obvious that there is very good agreement with experimental data for both, the calculated CDDs and charge form factors.

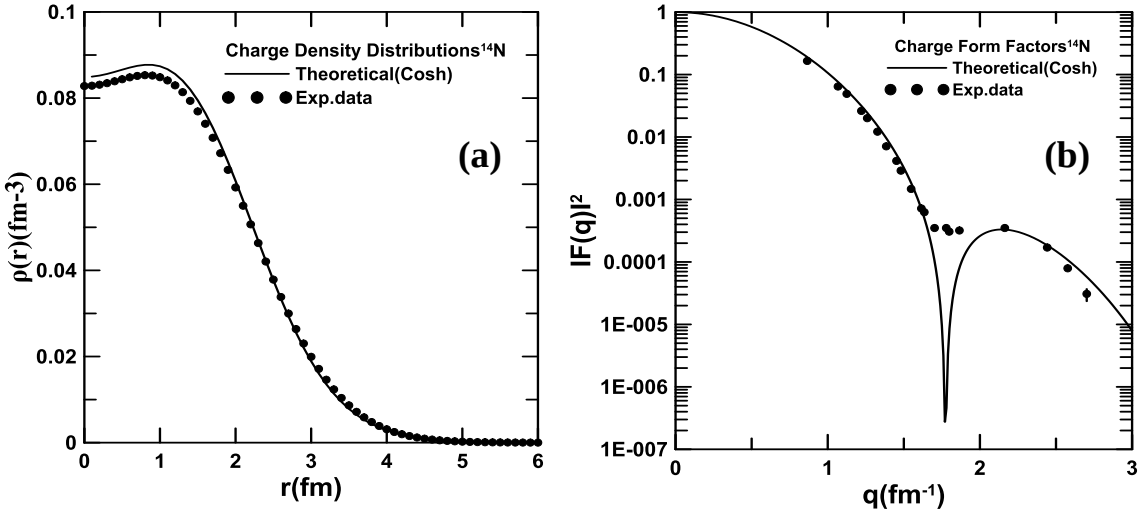

Figure 1- (a) Calculated CDD for ^{14}N are illustrated and compared with experimental data [16]. In (b), the calculated charge form factors are depicted and compared with experimental data of ^{14}N [24].

The calculated MDDs for ^{16,18}N are drawn in Figure 2 and in Figure 3 for ^{20,22}N. The solid curves represent the calculations using Cosh potential and the dotted symbols are the experimental data. For $^{18,\ 22}$N, the pure $2s_{1/2}$ configuration is found to be in very good agreement with experimental data. While for ^{16,20}N, the pure $1d_{5/2}$ configuration is found adequate to make the calculation in very good agreement with experimental data for all. From Figures 3 and 4, it is clear that the asymptotic region of r for the calculated MDDs are well generated which is the main and outstanding feature of exotic nuclei.

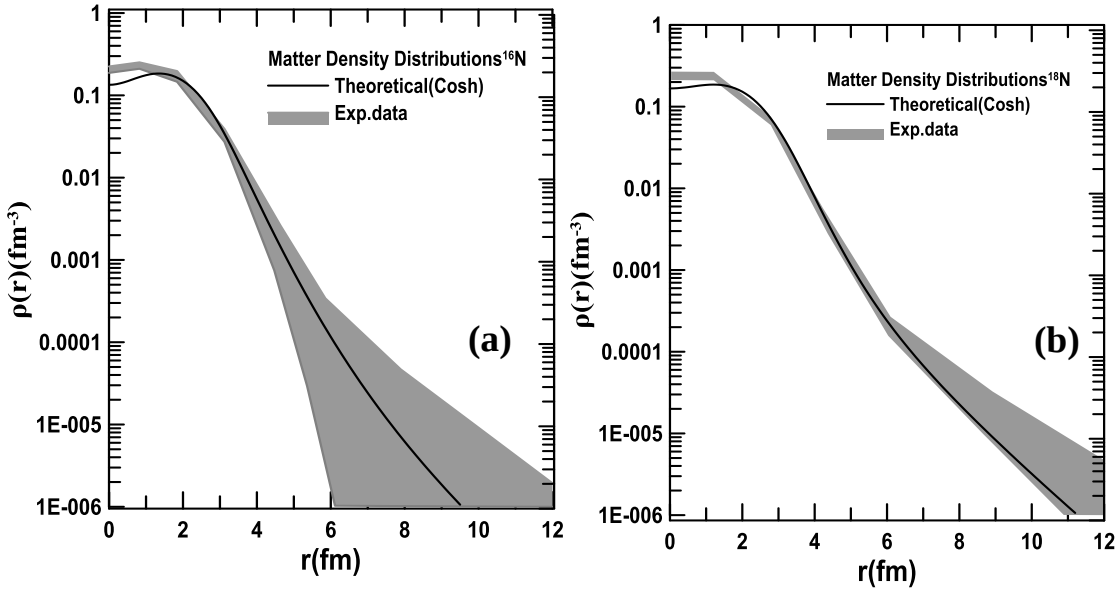

Figure 2- Calculated MDDs for ^{16}N (a) and ^{18}N (b) are depicted and compared with experimental data [25]. The pure $1d_{5/2}$ and $2s_{1/2}$ configurations for ^{16}N and ^{18}N, respectively are presumed.

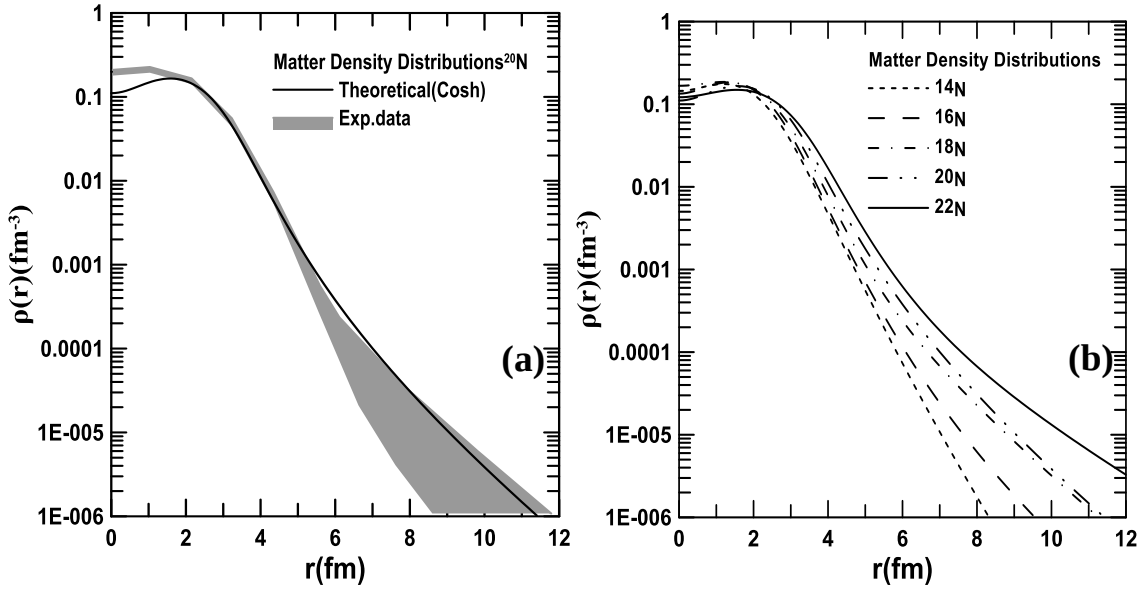

Figure 3- (a) Calculated MDDs for ^{20}N (a) and ^{22}N (b) are depicted and compared with experimental data [25]. The pure $1d_{5/2}$ and $2s_{1/2}$ configurations for ^{20}N and ^{22}N, respectively are presumed.

In Figure 4, the calculated MDDs for ^{14,16,18,20,22}N are gathered together for comparison. It is worth mentioning that with increasing neutron numbers, the single-neutron binding energy decreases and consequently the tunneling in the calculated MDDs increases, leading to the upwards shift for the MDDs.

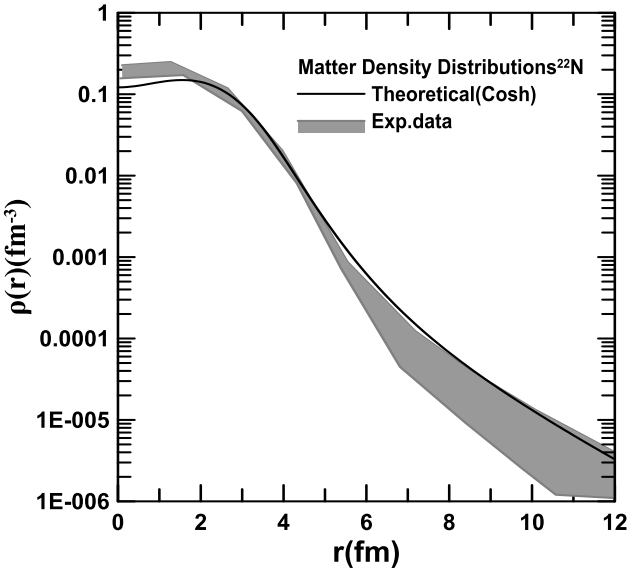

Figure 4- Calculated MDDs for ^{14,16,18,20,22}N are displayed for comparison.

In Figure 5, the calculated charge form factors for ^{16,18,20,22}N are all compared with the experimental data of ^{14}N. It is noticed that with increasing neutron numbers, the calculated ground charge form factors shift downwards and backwards in comparison with ^{14}N.

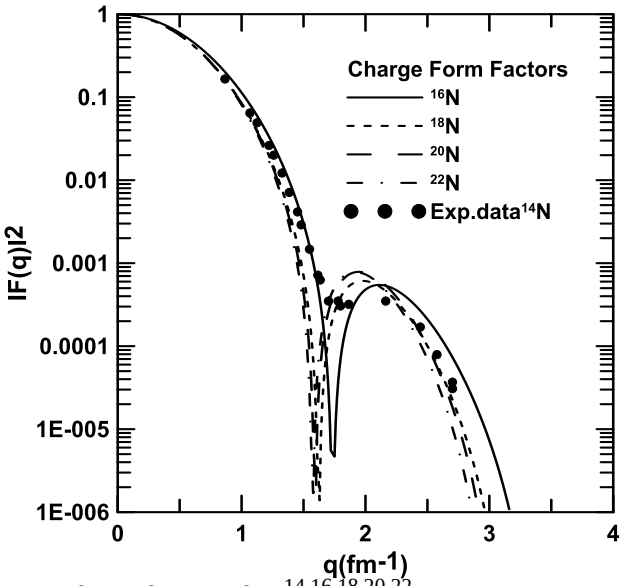

Figure 5- Computed charge form factors for ^{14,16,18,20,22}N are depicted and compared with the experimental data of ^{14}N [24].

Conclusion

The nuclear ground density distributions and electron scattering charge form factors for nitrogen isotopes ^{14,16,18,20,22}N have been computed using the bound radial wave functions of Cosh potential. The parameters of the aforementioned potential for the isotopes under study are set so as to reproduce the neutron and proton binding energies at Fermi's level, as well as the experimental size radii for each isotope under study. For the calculated ground state matter density distributions, it is found that the results are in a very good agreement with experimental data and greatly improved by using such potential, besides, the tail in calculated

densities are increased with the decreasing in the binding energies for the last single neutron on Fermi's level; and this is a result of high tunneling effect in the asymptotic part of the radial wave functions. Finally, for the calculated charge form factors, it is found that with increasing neutron numbers, the calculated charge form factors shifted backwards and downwards due the increasing in the screening effect coming from the increasing numbers in the neutrons.

Ref**erences**

[1] H. Uberall, "Electron Scattering From Complex Nuclei. Part A and B," Academic Press New York and London,**1971**.

[2] P. Navrátil and B. R. Barrett, "Large-basis shell-model calculations for p-shell nuclei," *Phys. Rev*. C**57**, pp. 3119-3128, **1998**.

[3] P. Navrátil and W. Erich Ormand, "Ab initio shell model with a genuine three-nucleon force for the p-shell nuclei," *Phys. Rev.* C**68**, 034305, pp. 1-13, **2003**.

[4] P. Navrátil, E. W. Ormand C. Etienne, and C. Bertulani, "No-Core Shell Model and Reactions," *AIP Conference Proceedings*, vol. **791**, pp. 32-39, **2005** .

[5] A. K. Hamoudi, R. A. Radhi and A. R. Ridha, "Theoretical study of matter density distribution and elastic electron scattering form factors for the neutron-rich ^{22}C exotic nucleus," *Iraqi Journal of Physics*, vol. **10**, pp. 25-34, **2012** .

[6] R. A. Radhi, A. K. Hamoudi, and A. R. Ridha, "Elastic Electron Scattering from Unstable-Neutron-Rich ^{19}C Exotic Nucleus," *Iraqi Journal of Science*, vol. **54**, pp. 324-332, **2013**.

[7] A. K. Hamoudi, R. A. Radhi and A. R. Ridha, "Elastic electron scattering from ^{17}Ne and ^{27}P exotic nuclei," *Iraqi Journal of Physics*, vol. **13**, pp. 68-81, **2015**.

[8] A. R. Ridha, M. K. Suhayeb, "Theoretical Study of Nuclear Density Distributions and Elastic Electron Scattering form Factors for Some Halo Nuclei," *Iraqi Journal of Science*, vol. **58**, pp. 2098-2106, **2017** .

[9] S. H. Mohammed and A. R. Ridha, "Theoretical Study of the Electromagnetic Structure of Boron Isotopes Using Local Scale Transformation Technique," *Iraqi Journal of Science,* vol. **59**, pp. 1866-1877, **2018**.

[10] S. H. Mohammed and A. R. Ridha, "Study of nuclear structure for carbon isotopes using local scale transformation technique in shell model," *Iraqi Journal of Physics*, vol. **16**, pp. 103-116, **2018**.

[11] A. R. Ridha, "Study of charge density distributions, elastic charge form factors and root-mean square radii for ^{4}He, ^{12}C and ^{16}O nuclei using Woods-Saxon and harmonic-oscillator potentials," *Iraqi Journal of Physics*, vol. **14**, pp. 42-50, **2016**.

[12] A. R. Ridha and Z. M. Abbas, "Study of matter density distributions, elastic charge form factors and size radii for halo ^{11}Be, ^{19}C and ^{11}Li nuclei," *Iraqi Journal of Physics*, vol. **16**, pp. 29-38, **2018**.

[13] R. I. Noori and A. R. Ridha, "Density Distributions and Elastic Electron Scattering Form Factors of Proton-rich ^{8}B, ^{17}F, ^{17}Ne, ^{23}Al and ^{27}P Nuclei," *Iraqi Journal of Science*, vol. **60**, pp. 1286-1296, **2019**.

[14] W. Greiner and J. A. Maruhn, "Nuclear Models," Springer-Verlag Berlin Heidelberg, **1996**.

[15] M. E. Grypeos, G. A. Lalazissis, S. E. Massen and C. P. Panos, "The cosh or symmetrized Woods-Saxon nuclear potential," *Journal of Physics G: Nuclear and particle Physics*, vol. **17**, pp. 1093-1105, **1991**.

[16] L. R. B. Elton, "Nuclear Sizes," Oxford University Press, **1961**.

[17] H. Chandra and G. Sauer, "Relativistic corrections to the elastic electron scattering from ^{208}Pb," *Phys. Rev.* C**13**, pp. 245-252, **1976** .

[18] M. Wang, G. Audi, A. H. Wapstra, F.G. Kondev, M. Mac Cormick, X. Xu and B. Pfeiffer, "The AME2012 atomic mass evaluation," *Chinese Physics* C**36**, pp. 1603-2014, **2012**.

[19] G. Audi, F. G. Kondev, W. J. Meng Wang and S. Huang Naimi, "Evaluation of nuclear Properties," *Chinese Physics* C**41**, 030001, pp. 1-138, **2017**.

[20] S. Bagchi, R. Kanungo , W. Horiuchi, G. Hagen, T.D. Morris, S.R. Stroberg, T. Suzuki, F. Ameil , J. Atkinson, Y. Ayyad, D. Cortina-Gil, I. Dillmann, A. Estradé, A. Evdokimov, F. Farinon, H.

Geissel, G. Guastalla, R. Janik, S. Kaur, R. Knöbel, J. Kurcewicz, Yu.A. Litvinov, M. Marta, M. Mostazo, I. Mukha, C. Nociforo, H.J. Ong, S. Pietri, Prochazka, C. Scheidenberger, B. Sitar, P. Strmen, M. Takechi, J.Tanaka, Y. Tanaka, I. Tanihata, S. Terashima, J. Vargas, H. Weick and J.S. Winfield, "Neutron skin and signature of the $N = 14$ shell gap found from measured proton radii of $^{17-22}$N," *Physics Letters* B**790**, pp. 251-256, **2019**.

[21] S. Ahmad, A. A. Usmani and Z. A. Khan, "Matter radii of light proton-rich and neutron-rich nuclear isotopes," *Physical Review* C**96**, 064602, pp. 1-13, **2017**.

[22] H. De Vries, C. W. De Jager and C. De Vries, "Nuclear charge density distribution parameters from elastic electron scattering," *Atomic Data and Nuclear Data Tables*, vol. **36**, pp. 495-536, **1987**.

[23] A. Ozawa, T. Suzuki and I. Tanihata, "Nuclear size and related topics," *Nuclear Physics* A**693**, pp. 32-62, **2001**.

[24] E. B. Dally, M. G. Croissiaux and B. Schweitz, "Elastic Electron Scattering Experiments with N^{15}," *Physical review* C**2**, pp. 2057-2068, **1970**.

[25] A. Ozawa, "Measurement of the interaction cross-section and related topics," *The European Physical Journal* A**13**, pp. 163-167, **2002**.